

The Potential of Cross-Stream Aligned Sub-Arrays to Increase Tidal Turbine Efficiency

S.C. Cooke^{a,1}, R.H.J. Willden^a, B.W. Byrne^a

^a*Department of Engineering Science, University of Oxford, Parks Road, Oxford OX1 3PJ, UK*

Abstract

A theoretical model is proposed for a row of sub-arrays of tidal turbines aligned in a cross-stream fashion across part of a wide channel. This model builds on previous work investigating the behaviour of a single partial row array that split the problem into two flow scales; device and channel. In the present work, three flow scales are proposed: device, sub-array and channel flow, allowing the mass, energy and momentum conservation balance to be assessed separately at each scale. The power potential of a row of sub-arrays with varying blockage ratios at each flow scale is investigated, and it is found that increasing device local blockage has the greatest potential to increase power yield. It is also found that, for such a single row tidal farm with a sufficient number of devices in a very wide channel, splitting the long fence array into multiple smaller co-linear sub-fences can increase the overall energy extraction potential. A new maximum power coefficient is found in infinitely wide flow, increasing from the Lanchester-Betz limit of 0.593 for turbines in unblocked flow, past the partial row array limit of 0.798, to a new limiting value of 0.865 for a row of multiple sub-arrays.

Keywords:

Tidal stream energy, Array, Actuator disc, Channel blockage

1. Introduction

There is much interest at present in the potential of tidal turbines to address the need for a renewable energy source which is reliable and predictable. In the UK, tidal stream energy is identified as a key constituent of marine energy development to meet the 2020 energy targets (Department of Energy and Climate Change, 2010) and there is considerable work being undertaken in the sector at present (Lawrence et al., 2013). In order to generate a significant amount of power, it is widely accepted that large numbers of turbines will need to be grouped together in arrays or farms, most likely at sites with tidal flow regimes which are best suited to energy extraction. The initial industry assumption was that such tidal turbine farms would be arranged with turbines working independently of each other as in a wind farm, however this

¹Email address for correspondence: susannah.cooke@eng.ox.ac.uk

neglects the differing flow regimes between the open atmosphere and a constrained tidal channel. Recent work has indicated that significant improvements in power extraction can be gained by capitalising on the effect of channel blockage, which causes the flow through the turbines and the bypassing flow to interact to enable greater pressure (static head) drop across the turbine, resulting in increased power extraction. This effect can be achieved by arranging turbines in long row arrays, and it has been found (Vennell, 2010, 2011) that in such cases the limiting maximum power which can be extracted from the free-stream energy flux can be significantly increased from that of a single turbine operating alone in unconstrained flow, known as the Lanchester-Betz limit, which is the applicable limit for a wind turbine.

The work of Lanchester and Betz in the early 20th century (Lanchester, 1915; Betz, 1920) derived an upper theoretical limit for power extraction from a turbine, equating to $16/27$ or 0.593 of the upstream kinetic flux. This work assumed an infinite flow field, which is a reasonable assumption for a wind turbine in the unconstrained atmosphere but is less well-suited to tidal turbines in the relatively constrained environment of coastal waters. When interest in tidal stream turbines began increasing in the late 20th century, estimates of available power were usually based on kinetic energy flux as in the wind industry (European Commission and Others, 1996), and this assumption continued to be used in detailed assessments of tidal resource as the first industrial-scale turbine installations in the UK were under discussion and development (Fraenkel, 2002; Black & Veatch, 2005).

With recent advances in tidal stream technology in the following decade, however, more realistic assessments of energy extraction have become necessary. Device designers can model an individual device in detail to develop its structural, hydrodynamic and electrical design, but the need to model large arrays of devices in real tidal channels at an appropriate level of complexity poses a significant challenge for the industry at present. Ideally, arrays of tens of turbines would be modelled using three dimensional blade-resolved simulations in domains containing the real bathymetry of a tidal site, with resolution sufficient to capture all wake mixing effects. At present, however, solving such a scenario would have an infeasibly high computational cost, particularly if an iterative solution to find optimal turbine design or siting was required. As such, a variety of different approaches to computational, experimental and theoretical array modelling have been investigated by various authors (Vennell et al., 2015), each making assumptions to allow these large-scale problems to be tractable.

One approach is to use a computational fluid dynamics code which solves the three-dimensional Reynolds-Averaged Navier-Stokes (RANS) equations, but to simplify the channel geometry and the turbine model; this often involves a rectangular channel and use of actuator models for the turbines, such as in Daly et al. (2013) and Hunter et al. (2015). It is also possible to simplify the turbine model using Blade Element Momentum (BEM) theory, which Malki et al. (2014) utilised to study the performance of staggered turbines in an array. However, the use of three-dimensional modelling of any kind significantly limits the number of devices which can be considered due to computational cost with expanding domain size. Experimental modelling of arrays

has been similarly restricted to studying the interaction of small numbers of devices at the largest possible Reynolds numbers achievable in existing facilities: for example, Stallard et al. (2013) studied a single row array of up to five scale rotors, while Myers and Bahaj (2012) considered three porous discs in a staggered row arrangement and Mycek et al. (2014) reported results for two axially aligned turbines, one behind the other.

In order to computationally study large scale resources with arrays of many tens of devices, it is necessary to significantly reduce the complexity of the problem. This can be done by using simplified numerical models in which individual turbines or arrays are represented as either enhanced friction terms or momentum sinks within a simulation of the two-dimensional shallow water equations (Draper et al., 2013; Walters et al., 2013). If sufficiently simplified, these models can be computationally efficient enough to allow optimisation of array layouts (Divett et al., 2013; Funke et al., 2014). It should be noted, however, that these models, being two-dimensional in nature, cannot capture the complete three-dimensional wake mixing effects, and as such are necessarily limited in their ability to simulate arrays with closely-spaced turbines where these effects are important, unless specifically accounted for through sub-grid models (Serhadhoğlu et al., 2013; Vogel et al., 2013).

In order to evaluate the outputs of resource modelling, it is necessary to understand the theoretical limits of energy extraction by arrays of devices within tidal channels, just as the Lanchester-Betz limit is used as a theoretical benchmark in wind turbine design. The simplest influence of channel blockage was accounted for in the theory model of Garrett and Cummins (2007), complementing their previous analytical model of available tidal power from the head-driven flow through a tidal channel (Garrett and Cummins, 2005). Later models such as that of Nishino and Willden (2012) and Draper and Nishino (2014) have extended this framework with additional degrees of complexity to allow consideration of arrays of multiple devices. This theoretical framework, focusing on simplified models of fluid flow to obtain maximum limits of energy extraction, has been developed over recent years as described in the following paragraphs.

Garrett and Cummins (2005) examined the energy balance of the flow through a tidal channel in order to predict the power available for extraction by tidal turbines. It was discovered that the maximum power available to be extracted by any device within it is not directly related to the kinetic flux through the channel, because of the constrained nature of the flow. Instead, by considering momentum balance within a constrained tidal channel, they developed an expression for maximum average power, P_{max} , available in terms of the tidal head, a , developed along a channel which has an undisturbed volumetric flux of Q_{max} :

$$P_{max} = \gamma \rho g a Q_{max} \quad (1)$$

where ρ is the density of sea water, g is acceleration due to gravity, and γ is in the range 0.2 - 0.24. This range of γ reflects uncertainty in the model regarding the appropriate drag law, contributions from bed

friction and channel exit effects, etc. This derivation considered the energy balance between the potential energy of the tidal head and the flow resistance due to the turbine and other effects such as bed friction. Their study assumed that the thrust of the tidal turbine was equally spread across the entire channel bed, i.e. that a turbine array completely filled the channel at one point along its length. In real channels, this is clearly not practical, and so Garrett and Cummins extended their work further by considering Linear Momentum Actuator Disc Theory (LMADT) to model flows through and around a single turbine in a constant mass flux channel (Garrett and Cummins, 2007).

Given that, in a real tidal channel, it is likely that tidal turbine arrays will only occupy a proportion of the channel’s cross-section, due to uneven bathymetry, turbine geometry, requirements for shipping channels and the like, this work has been further developed by many others, in different ways. Vennell combined the single turbine model with the variable channel flow model (Vennell, 2010) and showed that for a homogeneous turbine fence completely occupying the width of the channel, the optimal turbine through-flow varies depending on the proportion of the channel cross-sectional area filled by turbines. Highly blocked channels achieve maximum power output with greater flow induction through each turbine. A following study also showed that more power can be achieved by increasing the number of turbines in a single row than by creating additional rows of turbines (Vennell, 2011).

The single turbine model has several limiting assumptions, some of which were addressed by Whelan et al. (2009) and Housby et al. (2012) to allow more complex cases to be considered, in particular the case of open channel flow with a non-zero Froude number. This case is of particular interest where high channel blockage with a large number of turbines creates a significant flow obstruction and causes considerable head loss across the turbine fence.

The work of Nishino and Willden (2012) extended the single turbine model of Garrett and Cummins (2007) in a different direction to enable turbine fences of finite length, which do not completely occupy the width of the channel, to be modelled. Their work introduced the idea of scale separation to allow an entire row array to be modelled as one device in a channel, while all the turbines within the array are similarly modelled as devices within a separate array channel defined by the array core flow properties. This model maintained the assumptions of constant mass flux and constrained (rigid lid) flow of Garrett and Cummins (2007), while introducing an additional assumption of scale separation between device scale and array scale wake mixing. This model predicted a maximum power coefficient for an infinitely wide channel of 0.798, a significant increase on the completely unconstrained Betz limit of 0.593. The assumption of complete scale separation was partially addressed in later work (Nishino and Willden, 2013) to include short row arrays with significant device wake expansion, and simultaneously validated with three-dimensional flow analysis which showed better agreement with partial row array model results than it did with the original single turbine Garrett and Cummins (2007) model.

The present paper will extend the model of Nishino and Willden in a different direction, proposing a

112 further level of scale separation to investigate the potential for splitting a long row array of turbines into
 113 smaller sub-arrays, still arranged in a row. As such, a review of previous LMADT modelling will first be
 114 provided, followed by the details of the new sub-array model. The results obtained from this model will
 115 then be presented and discussed.

116 2. LMADT Turbine and Array Modelling

117 In order to create a model of sub-arrays within a wider cross-stream ‘farm’ row across a channel, it is
 118 necessary to build up the analytical flow equations from the original single turbine model of Garrett and
 119 Cummins (2007).

120 2.1. Single Turbine

121 A single device in a channel is shown in Figure 1, with the channel, device and bypass flow speeds
 122 (designated by U_C , U_D and U_B respectively) shown at various locations along the channel axis in terms of
 123 the device and wake induction factors, α and γ . The locations correspond to positions of interest within the
 124 channel such that position 1 is the upstream undisturbed flow, where velocity and pressure are equal across
 125 the channel, while positions 2 and 3 immediately upstream and downstream of the turbine within the core
 126 flow witness the same flow speed. Wake expansion occurs prior to position 4 where pressure equalisation
 127 across the channel occurs, and position 5 is far downstream after all mixing events have occurred and velocity
 128 has equalised across the channel cross-section.

129 It should be noted that the device induction factor is alternatively denoted as a_L instead of α_L , where
 130 $a_L = 1 - \alpha_L$ such that:

$$U_D = \alpha_L U_C = (1 - a_L) U_C \quad (2)$$

131 The ‘local’ subscript L is introduced here to denote the channel flow immediately surrounding the device,
 132 as distinct from the array and tidal farm channels to be discussed later. It is also necessary here to introduce
 133 the concept of blockage, which is the proportion of the local channel taken up by the device. It should be
 134 noted that the analytical model as presented is a function of non-dimensional blockage and is not dependent
 135 on turbine form or channel shape. However, circular axial flow turbines and rectangular section channels
 136 are used to exemplify array configurations in this paper. The definition of blockage for such a turbine in a
 137 channel therefore becomes:

$$B_L = \frac{\pi d^2/4}{hw} \quad (3)$$

138 where d is the turbine diameter, and h and w are the channel height and local channel width respectively.
 139 Note that $0 \leq B \leq 1$ for all blockage ratios, since they denote a percentage blockage of the surrounding

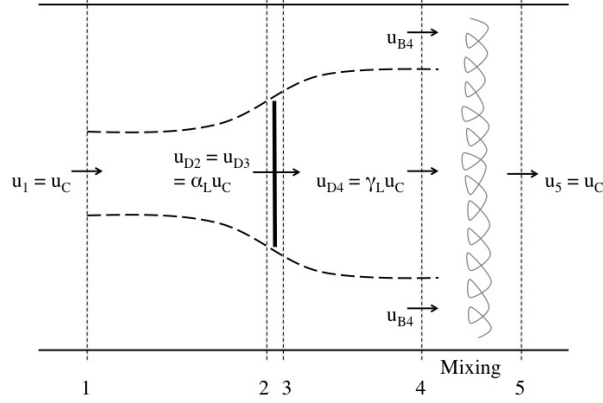


Figure 1: Schematic of a single device in a constrained channel.

channel. In particular, for the case of the local blockage ratio of a circular turbine within its local channel, this local blockage ratio can never exceed the area ratio of a circle in a square, i.e. 0.785.

Following Garrett and Cummins (2007) (see also Nishino and Willden (2012)), through consideration of the conservation of mass, momentum and energy at the positions noted along the length of the channel, it may be shown that a relationship for the local thrust coefficient as a function of the local channel induction factors:

$$C_{TL} = (1 - \gamma_L) \left[\frac{(1 + \gamma_L) - 2B_L(1 - a_L)}{(1 - (B_L/\gamma_L)(1 - a_L))^2} \right] \quad (4)$$

which in turn are related to each other through:

$$(1 - a_L) = \frac{1 + \gamma_L}{(1 + B_L) + \sqrt{(1 - B_L)^2 + B_L(1 - 1/\gamma_L)^2}} \quad (5)$$

The power output can be characterised in this model as

$$P_D = T_D U_D = T_D (1 - a_L) U_C \quad (6)$$

which through the standard definition of power coefficient gives

$$C_{PL} = \frac{P_D}{\frac{1}{2} \rho U_C^3 \pi d^2 / 4} = (1 - a_L) C_{TL} \quad (7)$$

and so it is possible to characterise the performance of the idealised turbine in terms of both power and thrust coefficients if either the device or wake induction factor is known (or assumed). In this way the performance of the device over a wide range of induction factors can be investigated for any given blockage ratio.

2.2. Partial Row Array

To create a model for a partial row array, following Nishino and Willden (2012), the single ‘device’ within the channel now becomes a row array, within which there are n local channels which operate in exactly the same fashion as each other. In each of these local channels there is a turbine, and the flow through the turbine can be characterised in the same way as in the Garrett and Cummins (2007) model, except that the upstream flow for each turbine local flow passage now becomes U_A - the flow speed approaching the array. The modelling scale separation assumption requires pressure equalisation and velocity recovery to occur homogeneously across all n local flow passages, well upstream of the point where array scale mixing commences. Hence, the velocities at the upstream and downstream turbine passage boundaries are both equal to U_A and provide a kinematic matching point to the array scale problem.

The channel characteristics at array scale, such as induction factors, are now denoted with an A subscript to separate them from the local characteristics specific to the turbine channel.

This results in new expressions for the flow speed and induction factors:

$$U_D = (1 - a_L)U_A \quad (8)$$

$$U_A = (1 - a_A)U_C \quad (9)$$

While local blockage is defined as the ratio of the area of the device under consideration at each scale to the area of the local turbine channel:

$$B_L = \frac{\pi d^2 / 4}{h(d + s_L)} \quad (10)$$

and array blockage as the ratio of array width to overall channel width:

$$B_A = \frac{n(d + s_L)}{w} \quad (11)$$

where s_L is the local spacing between each turbine within the array. The row array’s ‘area’ is taken to be its width (n times the diameter of the turbines plus the spacing between them) times the channel height, thus giving each turbine an individual channel of height h and width $d + s_L$.

As well as the local and array scale, a global scale is now introduced to relate directly from the devices to the global channel and as such represent the turbines’ performance in terms of the known upstream flow conditions. For example, the global induction factor, defining the flow speed through the device in terms of the upstream flow speed, becomes:

$$(1 - a_G) = \frac{U_D}{U_C} = \frac{U_D}{U_A} \frac{U_A}{U_C} = (1 - a_L)(1 - a_A) \quad (12)$$

It is then possible to consider conservation of mass, momentum and energy through each of the defined flow channels at local, array and global scale. The separate scales are related to each other through the kinematic matching of flow speeds as described above, as well as the fact that the total array thrust must equal the sum of the individual turbine thrust forces. As with the Garrett and Cummins (2007) single turbine model, this allows solution of the entire problem for thrust and power coefficients when the turbine’s local induction factor is specified.

3. Tidal farm model

There are limitations to the extensions to the partial row array model that are possible in terms of modelling different physical channel situations, given the assumptions made regarding the flow within each theoretical channel. For example, each channel’s bypass flow is treated as one single body of water, so that it cannot represent any asymmetrical positioning of devices within a channel, which may physically create pressure or flow speed imbalances within the bypass flow. However, a further extension of the model is possible to represent the realistic case of a single row of turbines clustered into several smaller sub-arrays. Thus, we consider an additional degree of scale separation, to allow for the situation where a very long row of turbines within a wider channel is split into m large sub-arrays, but still arranged in a cross-channel row, as shown in Figure 2. This creates an additional enveloping channel at the ‘farm’ level which can be analysed in the same fashion, much as the ‘partial row array’ model of Nishino and Willden (2012) created the outer array channel housing the inner turbine channel model.

In this problem, the flow field is considered at the local, array and farm scales. The local channel is the envelope immediately surrounding each device, as in the partial row array model previously described. The array channel contains a single sub-array and half the spacing to each of the two neighbouring sub-arrays, analogously to the definition of the device channel within the array. The farm channel is then the full channel, where the entire farm of sub-arrays now partially fills the whole channel and is treated as the ‘device’ at this scale.

If n is sufficiently large, all device-scale flow events around the turbine will occur much faster than the array-scale events around them, and if m is sufficiently large the same will be true for the array scale flow events and the global channel flow around them. This allows each scale of channel to be considered as a separate version of the single device Garrett and Cummins (2007) channel, whereby all mixing occurs before the flow equalises to that channel’s inlet velocity (i.e. position 5 for the local or array channel) and forms the device exit flow at the next channel scale (i.e. position 3 for the array or farm scale channel), where pressure equalisation and mixing at that scale then commence. Kinematic compatibility between scales is provided by this full velocity recovery within each problem scale such that the channel scale velocity, U_C , is seen upstream and downstream of the farm scale, the farm scale velocity, U_F upstream and downstream of

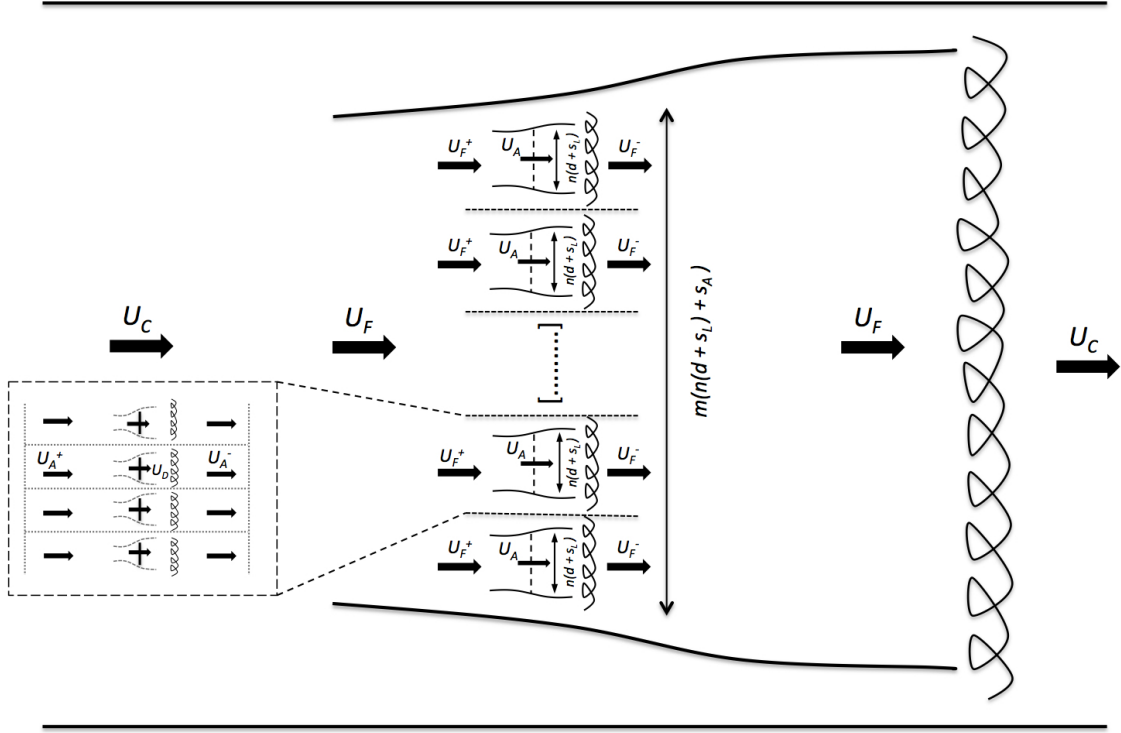


Figure 2: Example of a tidal farm layout with sub-arrays arranged in a row, showing device and sub-array channel scales. Superscripts + and - on flow speeds are included to show the recovery of the local channel speed from upstream to downstream of each scale of device.

each sub-array, and the array scale velocity, U_A , upstream and downstream of each device.

Thus induction factors are redefined at each scale:

$$U_D = (1 - a_L)U_A \quad (13)$$

$$U_A = (1 - a_A)U_F \quad (14)$$

$$U_F = (1 - a_F)U_C \quad (15)$$

where the subscript F denotes the farm scale. The local, array and farm blockage ratios within this model are defined as

$$B_L = \frac{\pi d^2/4}{h(d + s_L)} \quad (16)$$

$$B_A = \frac{n(d + s_L)}{n(d + s_L) + s_A} \quad (17)$$

$$B_F = \frac{m(n(d + s_L) + s_A)}{w} \quad (18)$$

where s_A is the spacing between sub-arrays, analogous to the local spacing s_L between turbines.

It is also now useful to define the global induction factor and blockage ratio, relating the turbine local fluid flow and turbine geometry to the overall channel characteristics:

$$(1 - a_G) = \frac{U_D}{U_C} = \frac{U_D}{U_A} \frac{U_A}{U_F} \frac{U_F}{U_C} = (1 - a_L)(1 - a_A)(1 - a_F) \quad (19)$$

$$B_G = \frac{mn\pi d^2/4}{hw} = B_L B_A B_F \quad (20)$$

As before, following the work of both Garrett and Cummins (2007) and Nishino and Willden (2012), the equations of conservation of mass, momentum and energy along the channels at each scale can be combined to obtain the array and farm thrust coefficients as functions of the induction factors and blockage ratios at each scale, as well as the relationship between the induction factors. These equations are copies of equations (4) and (5) for each of the other scales of channel:

$$C_{TA} = (1 - \gamma_A) \left[\frac{(1 + \gamma_A) - 2B_A(1 - a_A)}{(1 - (B_A/\gamma_A)(1 - a_A))^2} \right] \quad (21)$$

$$C_{TF} = (1 - \gamma_F) \left[\frac{(1 + \gamma_F) - 2B_F(1 - a_F)}{(1 - (B_F/\gamma_F)(1 - a_F))^2} \right] \quad (22)$$

$$(1 - a_A) = \frac{1 + \gamma_A}{(1 + B_A) + \sqrt{(1 - B_A)^2 + B_A(1 - 1/\gamma_A)^2}} \quad (23)$$

$$(1 - a_F) = \frac{1 + \gamma_F}{(1 + B_F) + \sqrt{(1 - B_F)^2 + B_F(1 - 1/\gamma_F)^2}} \quad (24)$$

The key relationship which allows all these equations to be solved is the fact that the total thrust at all scales must be the same. This allows the thrust coefficients at each scale to be related to each other through geometry and velocity (in which q denotes the dynamic pressure):

$$C_{TL} = \frac{\text{Thrust on single device}}{\text{Local inlet } q \times \text{single device area}} = \frac{T_D}{\frac{1}{2}\rho U_A^2 \pi d^2/4} \quad (25)$$

$$\begin{aligned} C_{TA} &= \frac{\text{Thrust on single array}}{\text{Array inlet } q \times \text{array frontal area}} \\ &= \frac{nT_D}{\frac{1}{2}\rho U_F^2 hn(d + s_L)} = (1 - a_A)^2 B_L C_{TL} \end{aligned} \quad (26)$$

$$\begin{aligned}
C_{TF} &= \frac{\text{Thrust on entire farm}}{\text{Channel inlet } q \times \text{farm frontal area}} \\
&= \frac{mnT_D}{\frac{1}{2}\rho U_C^2 h m(n(d + s_L) + s_A)} = (1 - a_F)^2(1 - a_A)^2 B_A B_L C_{TL}
\end{aligned} \tag{27}$$

Considering the entire channel, it is also possible to define thrust and power coefficients at the global scale, which relate total thrust and power to the upstream channel inlet flow speed and total device frontal area:

$$C_{TG} = \frac{mnT_D}{\frac{1}{2}\rho U_C^2 mn\pi d^2/4} = (1 - a_A)^2(1 - a_F)^2 C_{TL} \tag{28}$$

$$C_{PG} = \frac{mnT_D U_D}{\frac{1}{2}\rho U_C^3 mn\pi d^2/4} = (1 - a_L)(1 - a_A)^3(1 - a_F)^3 C_{TL} \tag{29}$$

The above relationships (26) and (27) between the thrust coefficients form the link between the different scales of the model. Substitution of the three thrust coefficient equations (4), (21) and (22) into these equations yields array and farm scale relationships between the axial and wake induction factors. Given that these induction factors are already related to each other through equations (23) and (24), it is therefore possible to solve the simultaneous equations for α_L and γ_L , and subsequently for α_A and γ_A . It should be noted that although equation (27) appears to create a direct link between the device-scale and farm-scale problems, the array-scale problem must still be solved because the array-scale induction factor a_A is still required in this equation and cannot be analytically determined.

All of the above equations can thus be solved, either analytically or numerically, for a given value of either a_L (or equivalently γ_L), which is a function of device design and operation. For each possible combination of blockage ratios, there will be an optimal axial induction factor, relating to an unspecified optimal design, which will result in maximum C_{PG} . This theoretical maximum may be found by considering an appropriate range of induction factors.

4. Results

Within the model described above, there are four independent variables which can be set to explore different scenarios: three blockage ratios and an induction factor. The model is then solved numerically to obtain all power and thrust parameters of interest. This results in a large parameter space which is best understood by considering specific different scenarios as outlined below, each of which represents a particular design case where this model would be relevant.

4.1. Fixed Array

The simplest case to consider is that of an array where the geometry of the array layout and the basic turbine design have already been developed, such that all blockages are fixed. The only variable remaining is

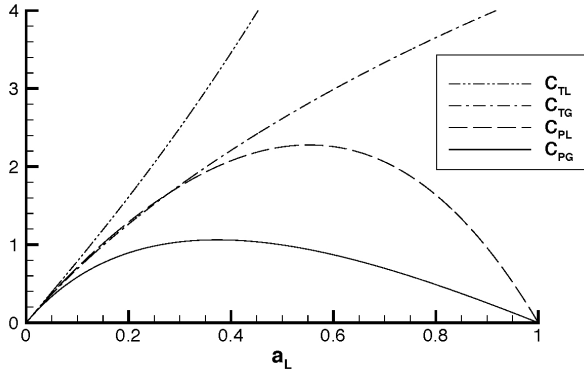


Figure 3: Variation of C_{TL} , C_{TG} , C_{PL} and C_{PG} with a_L , for $B_L = 0.49$, $B_A = 0.61$, $B_F = 0.44$ and $B_G = 0.131$.

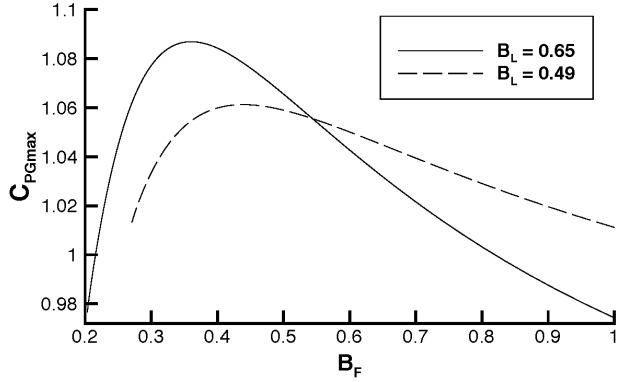


Figure 4: Variation of maximum C_{PG} against B_F , for fixed $B_G = 0.131$, showing cases of fixed $B_L = 0.65$ and $B_L = 0.49$.

the turbine induction factor, representing the ability to tune turbine performance in such a case (assuming that all turbines are tuned to the same induction factor). It is therefore possible to plot the maximum power coefficient that such an array can achieve against the local turbine induction factor.

This relationship, together with those for C_{PL} , C_{TL} and C_{TG} is shown in Figure 3 for a specific case where $B_L = 0.49$, $B_A = 0.61$, $B_F = 0.44$ and thus $B_G = 0.131$. For this specific selection of blockage ratios, it can be seen that C_{PL} peaks at a higher value of a_L than C_{PG} . This is due to the fact that at higher a_L , i.e. greater flow resistance through the turbines, C_{TL} increases significantly. This decreases flow speeds through the turbines and so reduces the total power coefficient based on global channel flow speed, C_{PG} . This is similar to previous results by e.g. Nishino and Willden (2012) for a partial row array.

4.2. Fixed Global Blockage

Another realistic scenario for tidal array development is that of an array where site selection has been completed and investment has been secured, effectively prescribing the number and size of the turbines. With this knowledge of total turbine frontal area and channel cross-sectional area, the global blockage ratio is fixed. However, local, array and farm blockages can still be varied based on the design of the turbines, their support structures and the overall proportion of the channel to be used. We consider the specific case of $B_G = 0.131$, as considered by Nishino and Willden (2012), which could equate to a tidal farm of ten arrays of ten 20m diameter turbines in an 8km wide channel with 30m depth.

In Nishino and Willden's partial fence model, at this level of global blockage, it was found numerically that maximum power was available when $B_L = 0.49$. This can be replicated within the farm model as the case where $B_A = 1$ and all arrays are joined end-to-end to create one single partial row array. Doing so produces identical results to the Nishino and Willden (2012) model at this value of local blockage. Retaining the same local blockage, but moving the arrays apart to increase farm blockage (and decrease array blockage),

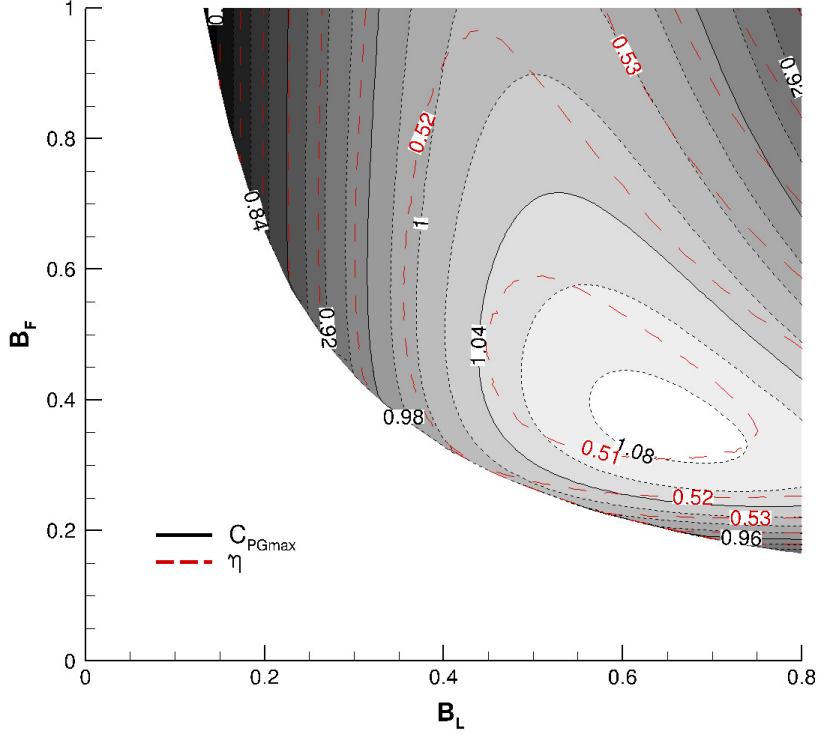


Figure 5: Contours (in greyscale) of maximum C_{PG} for a range of B_F and B_L , for fixed B_G of 0.131. Dashed red contours overlaid show corresponding basin efficiency η .

produces an increase in the maximum global power available, as can be seen in Figure 4.

Also shown in Figure 4 is a similar power curve for the case of $B_L = 0.65$, which at this global blockage corresponds to the maximum C_{PG} available within the farm model. (See later discussion of Figure 5.) This local blockage ratio would represent an ‘over-blocked’ scenario in the partial row array model (where $B_A = 1$, so $B_F = 0.2015$). This can be seen from the fact that the maximum C_{PG} available at this lower bound is significantly below that at the lower bound of the $B_L = 0.49$ case that resulted from the partial fence model (here, $B_A = 1$ corresponds to $B_F = 0.2673$). This is due to the fact that, in a continuous partial fence with a local blockage of 0.65, the increased resistance of the array blocks the flow and reduces power output. It can be seen that moving the sub-arrays apart and allowing internal bypasses between sub-arrays very quickly increases the power output and eventually allows the farm to achieve greater power than was possible with a continuous array, for both the $B_L = 0.49$ and $B_L = 0.65$ cases. Note that the scenario of fixed B_L and B_G is one of a fixed device design and a fixed number of devices available for deployment in a known channel and therefore represents a realistic scenario in which the design variables are the spacing between sub-arrays and the tuning of the turbines (determining B_F and α_L).

If local blockage is allowed to take any value, the surface of maximum achievable power coefficient at all possible B_L , B_A and B_F is shown in Figure 5. Each point in this plot represents the maximum C_{PG} at a specific blockage combination for any α_L , i.e. the peak value of the Figure 3 equivalent at every point. While B_A is not shown explicitly in this plot, it is determined at each point because it is inversely related to B_L and B_F , as they are related through (20) and B_G is constant. The curved lower boundary shows where $B_A = 1$, i.e. along this line the sub-arrays meet with no array bypass flow between them and the model reduces to the single partial row array model of Nishino and Willden (2012) .

It can be seen that for the given global blockage of 0.131 it is possible to increase C_{PG} from the partial row array model maximum of 1.011 to a new maximum of 1.087, i.e. a 7.5% increase. The increase in maximum C_{PG} when sub-arrays are allowed is achieved by increasing the local blockage ratio from 0.49 to 0.65 and spacing out sub-arrays such that the farm spreads from occupying 27% of the overall channel width to occupying 0.36 of it. If such a high local blockage is not achievable, however, it should be noted that even with the local blockage optimised for the Nishino and Willden (2012) partial row array model at 0.49, it is still possible to increase C_{PG} by 5% as shown in Figure 4 merely by breaking the continuous fence into sub-arrays, decreasing B_A and increasing B_F so that the farm covers 44% of the channel (up from 27%). This corresponds to moving vertically up the plot from the $B_A = 1$ lower boundary at $B_L = 0.49$. At low values of B_L , there is very little variation in C_{PG} , but where higher local blockage is possible then the use of sub-arrays can achieve significant gains in extractable power.

It is clear when considering the form of the C_{PG} plots and their maxima at any level of global blockage that there is a hierarchy of which blockage is most important for power output. The point of maximum power for $B_G = 0.131$ occurs at $B_L = 0.65$, $B_A = 0.56$ and $B_F = 0.36$. This pattern of $B_L > B_A > B_F$ at C_{PGmax} is repeated at all global blockages considered. This shows that local blockage is the most important to increase power output, supported by lower surrounding blockages at the array and farm scales.

While C_{PG} is an important measure of the potential power extraction that a tidal farm can achieve in a given location, it may also be important to consider the basin efficiency η , which is the ratio of power extracted by the turbines to total energy removed from the flow due to their presence. Within this model, the basin efficiency is related only to the global induction factor a_G :

$$\eta = \frac{\text{power extracted}}{\text{power removed}} = \frac{mnP_D}{mnT_D U_C} = \frac{U_D}{U_C} = (1 - a_G) \quad (30)$$

The basin efficiency achieved at the point of maximum C_{PG} is also shown in Figure 5 as a function of B_L and B_F . The contours of basin efficiency show that, in general, basin efficiency decreases as extractable power is increased. Since power and thrust are directly related through channel flow speed in this model, the point of maximum farm power equals the point of maximum farm thrust, which contributes to low basin efficiency by increasing the difference between core and bypass flow speeds at each scale. Increased

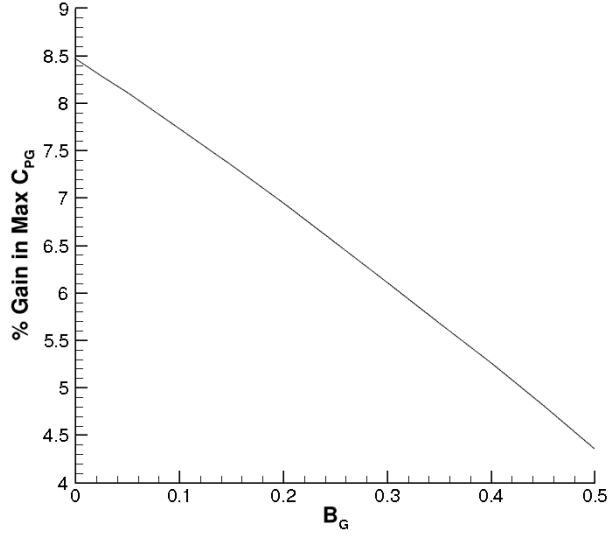


Figure 6: Potential % gain in maximum C_{PG} possible in moving from partial row array model to farm row model, for a range of B_G .

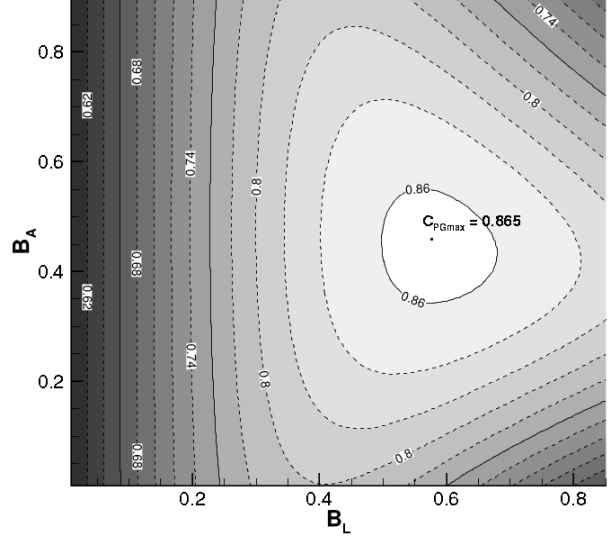


Figure 7: Contours of maximum C_{PG} for an infinitely wide channel ($B_F = B_G = 0$).

flow speed differentials lead to increased shear between the bypass and core flows, causing greater energy dissipation at the boundary and thus reducing basin efficiency as this energy is lost from the flow. However, it should be noted that the lowest values of η do not completely correspond with the highest values of C_{PG} , and so it would be possible to achieve a compromise situation with a relatively high power coefficient which would avoid the worst energy losses for the channel as a whole. This could be important where channels are likely to contain more than one tidal turbine farm along their length, to ensure there is as much energy as possible remaining in the flow after it passes the upstream farm. It can also be seen that it is possible to increase farm output power without reducing basin efficiency: for example, following the $\eta = 0.52$ contour to the right from the curved $B_A = 1$ boundary tracks up the contours of C_{PG} while retaining the same basin efficiency. In doing so, B_F , i.e. total width of fence, remains approximately constant. This physically corresponds to taking a partial row array and splitting it into sub-arrays by increasing B_L , i.e. bunching turbines more closely together to open up bypass flows between sub-arrays.

Note that the efficiency at maximum C_{PG} , $\eta = 0.51$ (i.e. $a_G = 0.49$), falls far below that anticipated by unblocked Lanchester-Betz type theory, for which $\eta = 2/3$ ($a_G = 1/3$) at maximum turbine efficiency.

4.3. Effect of Global Blockage

Figure 6 shows an exploration of the potential of this tidal farm arrangement of turbines to improve power output, for varying levels of global blockage within a channel. It starts from the position of the partial row array model, and shows the percentage increase in maximum possible C_{PG} when moving to the farm model, i.e. splitting up the long array to form sub-arrays. This potential increase in available power

is shown over a range of global blockage, assuming all other blockages are free to take any value in order to achieve C_{PGmax} . It can be seen that the potential to exploit the tidal farm model and gain increased available power by creating a sub-array structure is highest at low global blockages. It should also be noted that the model as a whole is less likely to accurately reflect real channel flow at high global blockage, as the constant mass flux and rigid lid assumptions are less likely to remain true, and thus a limit of $B_G = 0.5$ is used for this analysis. (It should be noted that the percentage gain in available power continues to decrease within the model at values of $B_G > 0.5$. However, regardless of the flow assumptions, geometric constraints mean that it is unlikely that this value will ever be exceeded in a real channel.) However, at low global blockage it can be seen that there is significant potential to increase power output merely through the creation of sub-arrays, possibly in the order of 5-8%.

4.4. Infinite Width Channel

It is finally of particular interest to consider the case of an infinitely wide channel, where $w \rightarrow \infty$ and $B_G \rightarrow 0$ (as $B_F \rightarrow 0$), and the far field effects of the tidal farm become negligible. For tidal turbines, which exist in a constrained medium, this case is analogous to the wind turbine in free atmosphere, where the Lanchester-Betz limit of 0.593 is the maximum power coefficient achievable. For the partial row array model, Nishino and Willden (2012) found a limiting maximum power coefficient for the infinite channel width case of 0.798, where the local blockage contributed to increase the extractable power. Both of these cases can be seen within the parameter space shown in Figure 7. The Betz limit is seen at the graph's origin, where $B_L = B_A = 0$, and the partial row array limit occurs where the highest value of C_{PG} is found along the B_L axis (where $B_A = 0$).

Allowing both B_L and B_A to vary in the tidal farm model, the limiting value of C_{PGmax} as $B_F \rightarrow 0$ is found to be 0.865, a more than 8% increase over the partial row array case. As was the case at non-zero global blockage, this is achieved at a higher local blockage than that of the partial row array C_{PGmax} .

5. Discussion

The results presented in this paper show that there is potential to optimise tidal turbine power yield through the careful choice of turbine and array spacing when turbines are arrayed in a row across a wide channel. The above analysis assumes that actuator discs are perfect energy extractors and as such it is not expected that the theoretical power maxima presented above could actually be reached by a real turbine farm. Further, the assumptions in the model require array widths and channels much larger than are currently under consideration for any tidal power installation. In particular, the assumption that all wake mixing events at each scale take place within that scale well prior to initiation of wake mixing at the wider scales results in a very long overall channel length required to permit this assumption, potentially longer

than most channels in which such a large tidal farm could be placed. The computational work of Nishino and Willden (2013) to validate the partial row array model showed that, although maximum theoretical values of C_{PG} as predicted by their partial fence model were not achieved in the computational simulation, the shape of the performance curves generally agreed and showed maxima at similar points. The computational results were also much closer to the partial row array model predictions than to the simple single device model of Garrett and Cummins (2007), showing that the theoretical device-channel scale separation did reflect a dominant part of the flow behaviour. It is therefore thought likely that in the new farm model, when introducing an additional such layer of scale separation, the gains in available power in moving from a continuous array to multiple sub-arrays are also real and achievable, even if real effects render those gains less than the analytic model might suggest.

This model does not consider many physical constraints which will affect the ability of a real tidal farm to achieve the blockages and power outputs predicted. The densest possible packing of circular, horizontal axis turbines within a channel the same depth as the turbine diameter is 0.785, which is not much greater than the optimal local blockages suggested by this model (0.65 for $B_G = 0.131$), and in practice would be difficult to achieve given bathymetry constraints and the natural change of channel depth over the tidal cycle. Even in the case where the local blockage remains the same, moving from one long partial row array of turbines to multiple sub-arrays in a row as posited here might, in real fluid flow, invoke losses due to array end effects on each of the sub-arrays. It should also be noted that increasing thrust to the level required to extract maximum power may reduce the flow rate through the channel, but this is dependent on each channel's characteristics; geometry, bed friction and tidal forcing.

It is suggested that most real tidal turbine installations will begin from a position of identifying a site and securing investment, effectively prescribing the number of turbines (or their total frontal area) and the channel dimensions, thus fixing global blockage. It is clear that the greatest potential for gains from creating sub-array rows comes in channels where there is reasonably low global blockage, although given the quasi-inviscid and scale assumptions within the model, these gains may not apply to small arrays in narrow channels. However, for larger installations in wide channels (but maintaining low global blockage), local, array and farm blockages will be determined following the selection of a site, based on device design and bathymetry constraints (B_L), support or sub-array design (B_A), and wider channel usage allowing for shipping lanes and other marine use (B_F). At this stage of development, the model shows that there is potential to improve power yield by considering blockage at all these scales before the tidal farm layout is fixed.

6. Conclusions

A new theoretical model has been proposed to investigate the efficiency of a long cross-stream tidal row array partially blocking a wide channel in depth-constrained flow, where the total array is comprised of multiple sub-array fences arranged in a single cross-stream row. This model creates three scales of fluid flow around the device, the sub-array and the tidal farm, in a manner similar to the two-scale ‘partial row array’ model of Nishino and Willden (2012). Assumptions are made to simplify the problem, as in the previous partial row array model: the flow is assumed to be quasi-inviscid, with a rigid lid and constant mass flux, and there is assumed to be scale separation between wake mixing effects at the three different scales.

The power that can be extracted from the flow is found to be maximised by careful selection of local, array and farm blockages, where high local blockage is found to be the most influential for increased power. The new model shows an increase in extractable power compared to the single fence ‘partial row array’ model of up to 8% at low global blockage. In the case of an infinitely wide channel, this increases the maximum power coefficient achievable from the Lanchester-Betz limit of 0.593 in unconstrained flow, past the Nishino & Willden partial fence maximum of 0.798, to a new theoretical maximum of 0.865.

This model provides a theoretical framework of a new mechanism to potentially increase tidal farm power. Further physical investigation is required to establish the practicalities of implementing this in a real tidal farm.

The authors wish to acknowledge the support of the EPSRC SuperGen UK Centre for Marine Energy Research (UKCMER).

References

- Betz, A., 1920. Das Maximum der theoretisch möglichen Ausnützung des Windes durch Windmotoren. *Zeitschrift für das gesamte Turbinenwesen* 26, 307–309.
- Black & Veatch, 2005. Phase II UK Tidal Stream Energy Resource Assessment. Carbon Trust Marine Energy Challenge .
- Daly, T., Myers, L., Bahaj, A., 2013. Modelling of the flow field surrounding tidal turbine arrays for varying positions in a channel. *Philosophical Transactions of the Royal Society of London A: Mathematical, Physical and Engineering Sciences* 371, 20120246.
- Department of Energy and Climate Change, 2010. Executive summary and recommendations. *Marine Energy Action Plan* 2010 .
- Divett, T., Vennell, R., Stevens, C., 2013. Optimization of multiple turbine arrays in a channel with tidally reversing flow by numerical modelling with adaptive mesh. *Philosophical Transactions of the Royal Society of London A: Mathematical, Physical and Engineering Sciences* 371, 20120251.
- Draper, S., Borthwick, A., Houlby, G., 2013. Energy potential of a tidal fence deployed near a coastal headland. *Philosophical Transactions of the Royal Society of London A: Mathematical, Physical and Engineering Sciences* 371, 20120176.
- Draper, S., Nishino, T., 2014. Centred and staggered arrangements of tidal turbines. *Journal of Fluid Mechanics* 739, 72–93.

European Commission and Others, 1996. Non-nuclear energy Joule II Wave Energy Project Results. The exploitation of tidal marine currents. European Commission DG Sci [Rep. EUR 16683 EN] .

Fraenkel, P.L., 2002. Power from marine currents. *Proceedings of the Institution of Mechanical Engineers, Part A: Journal of Power and Energy* 216, 1–14.

Funke, S.W., Farrell, P.E., Piggott, M., 2014. Tidal turbine array optimisation using the adjoint approach. *Renewable Energy* 63, 658–673.

Garrett, C., Cummins, P., 2005. The power potential of tidal currents in channels. *Proceedings of the Royal Society A: Mathematical, Physical and Engineering Science* 461, 2563–2572.

Garrett, C., Cummins, P., 2007. The efficiency of a turbine in a tidal channel. *Journal of fluid mechanics* 588, 243–251.

Houlsby, G.T., Draper, S., Oldfield, M.L.G., 2012. Application of Linear Momentum Actuator Disc Theory to Open Channel Flow. Technical Report OUEL 2296/08. Department of Engineering Science, University of Oxford.

Hunter, W., Nishino, T., Willden, R.H., 2015. Investigation of tidal turbine array tuning using 3d reynolds-averaged navier–stokes simulations. *International Journal of Marine Energy* 10, 39–51.

Lanchester, F.W., 1915. A contribution to the theory of propulsion and the screw propeller. *Journal of the American Society for Naval Engineers* 27, 509–510.

Lawrence, J., Sedgwick, J., Jeffrey, H., Bryden, I., 2013. An overview of the UK marine energy sector. *Proceedings of the IEEE* 101, 876–890.

Malki, R., Masters, I., Williams, A.J., Croft, T.N., 2014. Planning tidal stream turbine array layouts using a coupled blade element momentum–computational fluid dynamics model. *Renewable Energy* 63, 46–54.

Mycek, P., Gaurier, B., Germain, G., Pinon, G., Rivoalen, E., 2014. Experimental study of the turbulence intensity effects on marine current turbines behaviour. part ii: Two interacting turbines. *Renewable Energy* 68, 876–892.

Myers, L., Bahaj, A., 2012. An experimental investigation simulating flow effects in first generation marine current energy converter arrays. *Renewable Energy* 37, 28–36.

Nishino, T., Willden, R.H.J., 2012. The efficiency of an array of tidal turbines partially blocking a wide channel. *Journal of Fluid Mechanics* 708, 596–606.

Nishino, T., Willden, R.H.J., 2013. Two-scale dynamics of flow past a partial cross-stream array of tidal turbines. *Journal of Fluid Mechanics* 730, 220–244.

Serhadhloğlu, S., Adcock, T.A., Houlsby, G.T., Draper, S., Borthwick, A.G., 2013. Tidal stream energy resource assessment of the anglesey skerries. *International Journal of Marine Energy* 3, e98–e111.

Stallard, T., Collings, R., Feng, T., Whelan, J., 2013. Interactions between tidal turbine wakes: experimental study of a group of three-bladed rotors. *Philosophical Transactions of the Royal Society of London A: Mathematical, Physical and Engineering Sciences* 371, 20120159.

Vennell, R., 2010. Tuning turbines in a tidal channel. *Journal of Fluid Mechanics* 663, 253–267.

Vennell, R., 2011. Tuning tidal turbines in-concert to maximise farm efficiency. *Journal of Fluid Mechanics* 671, 587–604.

Vennell, R., Funke, S.W., Draper, S., Stevens, C., Divett, T., 2015. Designing large arrays of tidal turbines: A synthesis and review. *Renewable and Sustainable Energy Reviews* 41, 454–472.

Vogel, C.R., Willden, R.H.J., Houlsby, G.T., 2013. A correction for depth-averaged simulations of tidal turbine arrays, in: *Proceedings of the 10th European Wave and Tidal Energy Conference, Aalborg, Denmark*.

Walters, R.A., Tarbotton, M.R., Hiles, C.E., 2013. Estimation of tidal power potential. *Renewable Energy* 51, 255–262.

Whelan, J.I., Graham, J.M.R., Peiro, J., 2009. A free-surface and blockage correction for tidal turbines. *Journal of Fluid Mechanics* 624, 281–291.